Research on Seamless Image Stitching based on Depth Map

Chengming Zou, Pei Wu and Zeqian Xu
School of Computer Science and Technology, Wuhan University of Technology, Luoshi Road, Wuhan, China
{zoucm, wupei-pei}@whut.edu.cn, 937790017@qq.com

Keywords: Image Extraction, Image Stitching, Collaborative Calibration, Multi-band Blending.

Abstract: Considering the slow speed of panorama image stitching and the ghosting of traditional image stitching algorithms, we propose a solution by improving the classical image stitching algorithm. Firstly, a SIFT algorithm based on block matching is used for feature matching which was proposed in our previously published paper. Then, the collaborative stitching of the color and depth cameras is applied to further enhance the accuracy of image matching. Finally, according to a multi-band blending algorithm, we obtain a panoramic image of high quality through image fusion. The proposed algorithm is based on two problems in the technology of feature-based image stitching algorithm, the algorithm's real-time and ghosting. A series of experiments show that the accuracy and reliability of the improved algorithm have been increased. Besides a comparison with AutoStitch algorithm illustrates the advantage of the improved algorithm in efficiency and quality of stitching.

1 INTRODUCTION

Currently image stitching technology have achieved rapid development in many fields such as weather forecasting, space exploration, super resolution processing, reconstruction, military reconnaissance and digital cameras. The task of seamless image is to obtain a pair of high resolution panoramic images which are of big vision and no seam by processing a group of image sequence that have an overlapping area (Brown 1999).

A number of rsearchers have deeply studied about it. In the 1990s, Richard Szeliski (1996) proposed a mosaic model according to the camera's motion, which was processed by the iterative nonlinear minimization operator (Levenberg Marquardt, LM) to complete the image stitching. Based on the frequency domain characteristic of the image, two dimensional Fourier transform is used to solve the geometry transformation between different images and thus image mosaic is achieved. Jang(1999) implemented a panorama stitching algorithm based on equal match, the source image of which is photographed by rotating in the horizontal direction, so it doesn't apply in general situation. In 2003, Brown and Lowe proposed an image mosaic algorithm based on SIFT feature extraction, which had a huge impact in the field of image stitching. The algorithm is robust, and can automatically identify a plurality of view sand reject noise in the image. But its' camera model is so simple that it often affected by parallax and results in obvious ghosting. Wherein, SIFT algorithm was proposed in 1999 by them and further improved in 2004. The feature points acquired by SIFT operator are of scale and rotational invariant, which makes SIFT algorithm be widely used. In 2003, Mikolajczyk and Smith proposed an intelligent stitching algorithm on the basis of Szeliski's (2000) panoramic image stitching model. The algorithm can select a proper splicing model according to the camera's movement, which optimizes the efficiency and quality of image stitching. One year later, after more deep research, they improved the algorithm to intelligently select the best stitching model, which greatly enhanced the automation of the algorithm. Since then, adaptive issue has become a hot in the field of image stitching (Gholipour 2007, Brown and Lowe 2007). Brown and Lowe, who did further research to their previous work, implemented a panoramic image stitching image which can automatically stitch disorder images[10]. The algorithm used a probabilistic model to choose the images associated with the panoramic image from the disorder image sequence, thereby removing noise in the image and realizing panoramic stitching. In the early 10 years of the 21th century, J. Shin (2010) presented a new method of stitching binding the energy spectrum technology, which committed to

Zou, C., Wu, P. and Xu, Z.
Research on Seamless Image Stitching based on Depth Map.
DOI: 10.5220/0006146303410350
In *Proceedings of the 6th International Conference on Pattern Recognition Applications and Methods (ICPRAM 2017)*, pages 341-350
ISBN: 978-989-758-222-6

Algorithm 1: Seamless Mosaic Based on Depth map.

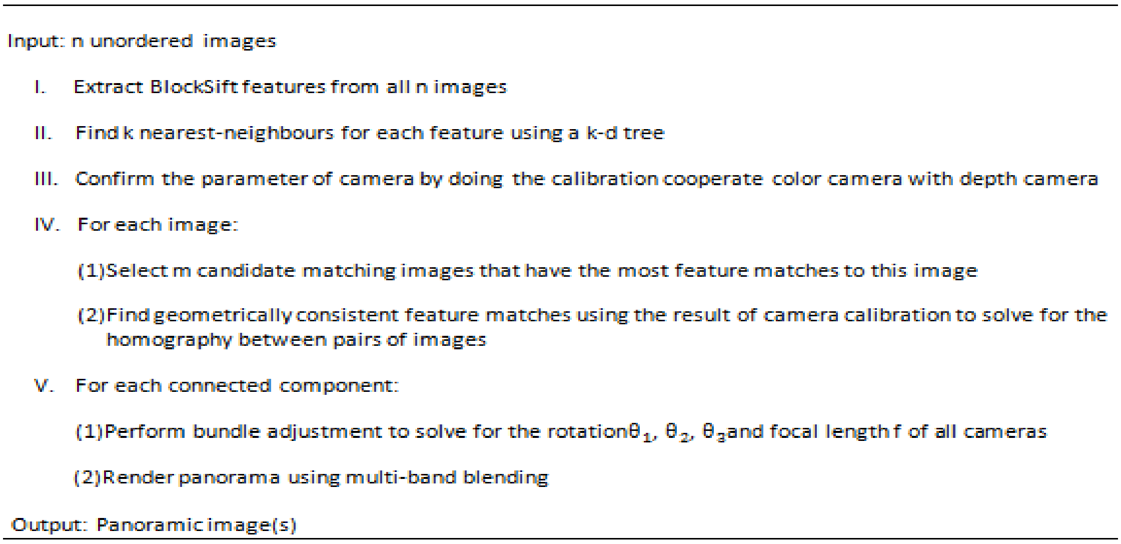

```
Input: n unordered images
    I.   Extract BlockSift features from all n images
    II.  Find k nearest-neighbours for each feature using a k-d tree
    III. Confirm the parameter of camera by doing the calibration cooperate color camera with depth camera
    IV.  For each image:
         (1)Select m candidate matching images that have the most feature matches to this image
         (2)Find geometrically consistent feature matches using the result of camera calibration to solve for the
            homography between pairs of images
    V.   For each connected component:
         (1)Perform bundle adjustment to solve for the rotation$\theta_1$, $\theta_2$, $\theta_3$and focal length f of all cameras
         (2)Render panorama using multi-band blending
Output: Panoramic image(s)
```

addressing the problem of ghosting. This algorithm achieved relatively good results but sacrificed in actual effect on a certain degree. Another important step in the process of image stitching, image fusion has huge influence to the quality of image stitching. The common mean of fusion is to fuse overlapping areas with weighted splicing operator, the main two methods of which are the cap-like function weighted approach and fade out and in weighted method (Gao 2011). The principle of the cap-like function is to spread to the surrounding pixels from the center of the overlapping area and make the weight descend (Singh 2007).

Through detailed research work, we found that the traditional stitching algorithms based on feature matching are robust, and they can successfully get the final mosaic images. However, there are two commonly problems. First, the speed of panorama image stitching is slow. Because the image stitching algorithms need to extract feature points towards all the images in the image sets, which will take a long time. Second, in the actual shooting process, there will be disparity which will increase the difficulty of image registration and cause significant ghosting.

Considering above two issues, we propose a solution by improving the classical image stitching algorithm. Firstly, a SIFT algorithm based on block matching is used for feature matching which was proposed in our previously published paper and proved to be robust(Zou 2015). And the detailed description can refer to reference 15. Then, the collaborative stitching of the color and depth cameras is applied to further enhance the accuracy of image matching. Finally, according to a multi-band blending algorithm, we obtain a panoramic image of high quality through image fusion. And the specific process of image stitching algorithm based on depth image is shown as algorithm1.

The proposed algorithm is based on two problems in the technology of feature-based image stitching algorithm, the algorithm's real-time and ghosting. A series of experiments show that the accuracy and reliability of the improved algorithm have been increased. Besides a comparison with AutoStitch algorithm illustrates the advantage of the improved algorithm in efficiency and quality of stitching.

2 COLLABORATIVE CALIBRATION BETWEEN THE DEPTHC CAMERA AND COLOR CAMERA

In Brown's and Lowe's experiment, they used a simple camera model, pinhole camera model, which didn't take some factors into consideration such as the geometric distortion of camera, the jitter and skew while screening. The parameters they used to describe the camera were so easy, so it may cause very serious ghosting. To solve this problem, we use a collaborative calibration between the color and depth cameras to align the depth camera to the color camera. After determining the internal and external parameters of those cameras, we can get the projection transformation matrix. The system uses a flat calibration method, and the steps are as follows.

2.1 Calibration

Depth camera can increase a channel to obtain the scene information for the computer. It is possible to build up the real-time three-dimensional scene through the real-time depth data of depth camera. However, in order to reconstruct a three-dimensional coordinate through the measured data of camera, the data in depth picture must to be aligned to the color pixels. And the process of alignment depends on the results of camera calibration. Because we can obtain the parameters through camera calibration which are necessary for alignment. Calibration includes the respective internal parameters and the external parameters between color and depth cameras. Color camera has been extensively studied. For depth camera, the existing research cannot meet the balance of accuracy and speed. And the results are easy to be influenced by the noise of depth data. In this case, we studied the joint calibration of color and depth cameras.

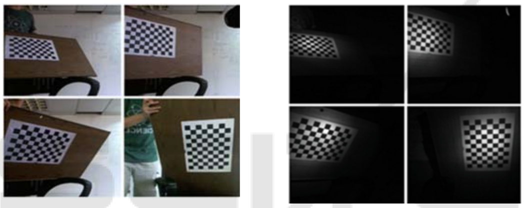

(a) (b)

Figure 1: Calibration of camera: (a) color camera and (b) depth camera.

To achieve the joint calibration of the color and depth cameras, we take the pictures of the checkerboard at different perspectives with the cameras to be calibrated, and calculate the matrix of the inner parameters of the camera and its outer parameters related to each image with the camera calibration interface provided by OpenCv library. Kinect depth camera uses an infrared speckle transmitter to emit infrared beam. Then when the light beam irradiates to the surface and reflects back to the depth camera, the depth camera will calculate the depth of the object through the geometric relationship between returning bulk spots. Figure 1 shows the calibration images of color camera and depth camera. And the right picture is the infrared figure corresponding to the color image. We can respectively calculate the internal parameters of the depth camera and color camera from Fig.1. Here, we use the interface provided by OpenCv to obtain the camera parameters. The distortion parameters of the color camera is [0.025163 -0.118850-0.006536-0.001345] and that of the depth camera is [-0.094718 0.284224 -0.005630-0.001429]. Then the internal parameters of the color camera and depth camera are:

$$\mathrm{E}_c = \begin{bmatrix} 554.952628 & 0.000000 & 327.545377 \\ 0.000000 & 555.959694 & 248.218614 \\ 0.000000 & 0.000000 & 1.000000 \end{bmatrix}$$

$$E_d = \begin{bmatrix} 597.599759 & 0.000000 & 322.978715 \\ 0.000000 & 597.651554 & 239.635289 \\ 0.000000 & 0.000000 & 1.000000 \end{bmatrix}$$

There are few points to be noted during the calibration. First, the calibration board should be as large as possible, at least to reach the size of A3 paper. Second, the angle between the board plane and the camera bead plane can't be too large, which should be controlled below 45 degrees. Third, the tilts and positions of the board need to be as diverse as possible, because those boards parallel to each other have no help to the calibration results. Fourth, there should be at least ten images used to calibrate, which can help to improve the accuracy. Fifth, the resolution of the camera should be properly set, and the aspect ratio is preferably the same as the depth map.

2.2 Projection Transformation Matrix

After the calibration of color camera, we need to obtain the projection transformation matrix, depth camera's internal parameters and outside parameters related to color camera.

In our calibration system, color camera is fixed on depth camera and they remain parallel. So we only need to do some certain translation transformation to project the depth data into the coordinate system of color camera. Then we need project the depth data into color image to form the final depth buffer. During the process, we must note that due to the different resolution of those two cameras, the depth buffer data and color data cannot be fully realized alignment in the strict sense, but we only need part of the depth data to verify, therefore, depth image need not be enhanced.

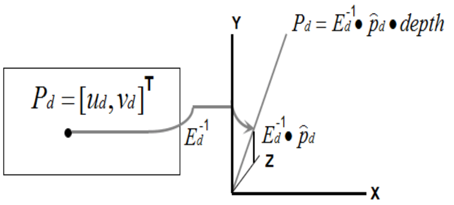
Y
$P_d = E_d^{-1} \bullet \hat{p}_d \bullet depth$
$P_d = [u_d, v_d]^T$
E_d^{-1}
$E_d^{-1} \bullet \hat{p}_d$
Z
X

Figure 2: The transformation from depth data to 3D coordinates.

On the corresponding area of the depth checkerboard image, we randomly calibrate a block regardless of the shape of it, but we must ensure that the number of pixel points is greater than ten. As Figure 2, for a pixel point on the block, α represents its disparity. And depth is got from (1), through which the back projection is achieved and converted to the 3 dimensional coordinate system to get the final 3D point p_d ($p_d = E_d^{-1} \cdot \hat{p}_d \cdot depth$).And $\hat{p}_d$ ($\hat{p}_d = [u_d, v_d, 1]^T$) is the homogeneous coordinate of p_d. After restoring the 3D coordinates for all the pixel points through their depth information, we can get the 3D point cloud.

$$depth = -\frac{0.075}{\tan(0.0002157a - 0.2356)}[m] \tag{1}$$

Then we need to calculate the projection matrix ${}^{D}T_C$. While converting its pixel point p_d to the color camera's coordinate, it can be expressed as $p_c^{'}$ ($\mathrm{p}_\mathrm{c}^{'} = {}^{D}T_C \cdot \hat{\mathrm{p}}_\mathrm{d}$). While the checkerboard is fit on the plate, the checkerboard acquired by color camera is on the same plane as that acquired by depth camera. That's to say that $p_c^{'}$ falls on the plane ofthe checkerboard acquired by color camera, so $\mathrm{p}_\mathrm{c}^{'}$ is fit to (2). Eliminating irrelevant variables, we can get equation as (3). For the point *j* in the sample *i*, we can get the equation as (4). p_{ij} is the plot of the $\hat{p}_d$ of point *j* in sample *i* and depth, and the vector can be calculated based on the sample. Besides $H = {}^{D}T_C \cdot E_d^{-1}$ represents the plot of the rotation matrix and translate vector matrix and the inverse of internal parameters matrix of depth camera.

$$r_{i3}^T \cdot p_c^{'} = \delta_{ic} \tag{2}$$

$$r_{i3}^T \cdot {}^{D}R_C \cdot E_d^{-1} \cdot \hat{p}_d \cdot depth + r_{i3}^T \cdot \ {}^{D}R_C = \ \delta_{ic} \tag{3}$$

$$r_{i3}^T \cdot H \cdot p_{ic} + r_{i3}^T \cdot {}^{D}t_C = \delta_{ic} \tag{4}$$

The process of establishing and solving equations is as follows:

$$\mathrm{H} = \begin{bmatrix} \mathrm{h}_1 & \mathrm{h}_2 & \mathrm{h}_3 \\ \mathrm{h}_4 & \mathrm{h}_5 & \mathrm{h}_6 \\ \mathrm{h}_7 & \mathrm{h}_8 & \mathrm{h}_9 \end{bmatrix}$$

$${}^{D}t_C = [t_1, t_2, t_3]^T$$

$$p_{ij} = [x_{ij}, y_{ij}, z_{ij}]^T$$

$$r_{i3} = [x_{i1}^{'}, x_{i2}^{'}, x_{i3}^{'}]^T A_{ij}^T = b_i$$

$$A_{ij}^T = b_i$$

Then A_{ij} is represented as (5) ($b_i = \delta_{ic}$). And $A_{ij}^T = \mathrm{b_i}$ is commonly replaced by (6). For M times' experiments with N_i points in each experiment, we can get (7). In this equation, a_{ij} represents the weight from this point to the equations. Through the least squares method we can get the value of *X*, and then get the value of Hand ${}^{D}T_C$.

$$A_{ij} = [\mathrm{x}_{ij}\mathrm{r}_{i1}^{'}, \mathrm{y}_{ij}\mathrm{r}_{i2}^{'}, \mathrm{z}_{ij}\mathrm{r}_{i3}^{'}, \mathrm{x}_{ij}\mathrm{r}_{i1}^{'}, \mathrm{y}_{ij}\mathrm{r}_{i1}^{'}, \mathrm{y}_{ij}\mathrm{r}_{i2}^{'}, \mathrm{z}_{ij}\mathrm{r}_{i3}^{'}, \mathrm{x}_{ij}\mathrm{r}_{i1}^{'}, \mathrm{y}_{ij}\mathrm{r}_{i2}^{'}, \mathrm{z}_{ij}\mathrm{r}_{i3}^{'}, \mathrm{r}_{i1}^{'}, \mathrm{r}_{i2}^{'}, \mathrm{r}_{i3}^{'}]^T \tag{5}$$

$$A_{ij}A_{ij}^T X = A_{ij}b_i \tag{6}$$

$$\sum_{i=1}^{M}\sum_{j=1}^{N_i}\left(a_{ij} \cdot A_{ij} \cdot A_{ij}^T\right) \cdot X = \sum_{i=1}^{M}\sum_{j=1}^{N_i}\left(a_{ij} \cdot A_{ij} \cdot A_{ij}^T\right) \tag{7}$$

Next we need to remove two types of noise, the one of which is generated by the change of the distance from depth camera to the object, while another of which is generated by the depth camera when acquiring depth images. Here we use the weight coefficient $\mathrm{a_{ij}} = \varphi_{\mathrm{ij}} * \emptyset_{\mathrm{ij}}$ to remove them.

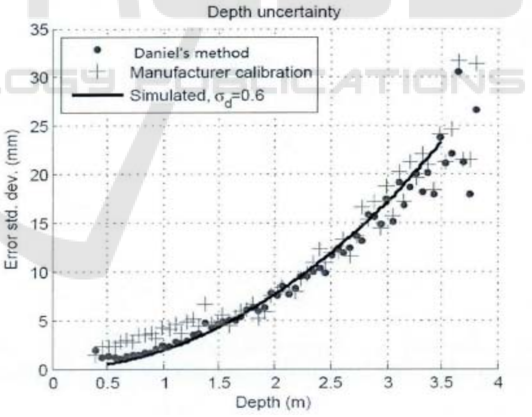

Figure 3: Solution of homography.

Kinect depth camera will produce noise along with the change of depth due to the principle of itself. Figure 3 shows the relationship between noise and depth, from which we can find that noise is proportional to the value of depth. So for t he depth data in different areas, we need to add different penalty coefficient, which is shown as (8).

$$\varphi_{ij} = \begin{cases} \dfrac{1}{1+\dfrac{1.2-depth}{0.6}} & if\ depth < 1.2 \\ 1 & if\ 1.2 \le depth \le 3.5 \\ \dfrac{1}{1+\dfrac{depth-3.5}{1.5}} & if\ depth > 3.5 \end{cases} \tag{8}$$

Through above steps, we have got the depth point cloud of the data of group i. Assuming that the equations of the plane is as $\mathrm{n}_\mathrm{i}^\mathrm{T} \cdot \mathrm{X} = \delta_\mathrm{i}$. $\mathrm{n}_\mathrm{i}$represents the normal vector of the flat plane, and δ_i represents vertical distance from t-he origin of camera coordinate to the flat. Suppose $\mathrm{P}_\mathrm{d}$is a point on flat. Because we have got the internal parameters matrix of kinect depth camera, $\mathrm{P}_\mathrm{d} = \mathrm{E}_\mathrm{d}^{-1} \cdot \hat{\mathrm{p}}'$. $\hat{\mathrm{p}}' = \hat{\mathrm{p}}_\mathrm{d} \cdot \mathrm{depth}$ represents the product of the depth and the 2D homogeneous coordinates of the pixel point on t-he area calibrated manually.$\mathrm{n}' = \mathrm{E}_\mathrm{d}^{-\mathrm{T}} \cdot \mathrm{n}$, so $\mathrm{n}'^\mathrm{T} \cdot \mathrm{p}' = \delta$. According to $\widehat{\mathrm{p}}'$, using Least Squares method to get n'^T . For the point p_j' on the area calibrated manually, $\varphi_\mathrm{ij}$can be defined as (9).

$$\varphi_{ij} = \begin{cases} 0 & if\ \left\| n'^T \cdot p_j' - \delta_i \right\| > 0.015 \cdot \delta_i \\ 1 & if\ \left\| n'^T \cdot p_j' - \delta_i \right\| \le 0.015 \cdot \delta_i \end{cases} \tag{9}$$

2.3 Homograph

Those associated images which are of overlapping area will be the source image of the panorama stitching. Because we have got the related blocks between the images, the matching relationship can be easily obtained with the related blocks. During the process of feature matching, we have got many matching relationship of feature points. Then, to achieve image stitch, we need obtain the homography matrix between stitching images by using the result of camera calibration, the internal control matrix of camera and the out parameters in relation to each image.

Homography refers to a reversible transformation from the real projective plane to the photography plane (Umeyama 1991, Chen 1994). In the domain of computer vision, any two images in the same space can be associated through homography (Triggs 2000).

We use the interface of OpenCV to solve the homography matrix, the principle of which is as follows. It calculates the rotation matrix and translation vector of each field of view by using the various images of a same project at different viewing angles. The rotation matrix and translation vector totally have six parameters, and the internal parameter matrix of the camera has four parameters. So, for each field of view, there are 6 non-constant parameters and 4 constant parameters needed to be solved. Mapping a square to a quadrilateral can be described with 4 two-dimensional points. Suppose that the vertex coordinates of the square on the physical plane is (u，v) and the coordinates of the related points on the imager is (x, y), the relationship between them can be described as (10) and (11). After substituting the coordinates of the four points into the above formulas in turn, we can get 8 equations. That's to say that a field of view of flat checkerboard can provide 8 equations. Therefore, it needs 2 fields of view (two images) to solve above 10 parameters. Besides, the points on the flat of original image are connected with the points on the aim flat through the (12) and (13). In addition, to achieve the process, OpenCV offers an interface of C function for the solving of homography.

$$u = f(x, y) \tag{10}$$

$$v = g(x, y) \tag{11}$$

$$p_{dst} = Hp_{src},\ p_{src} = H^{-1}p_{dst} \tag{12}$$

$$p_{dst} = \begin{bmatrix} x_{dst} \\ y_{dst} \\ 1 \end{bmatrix},\ p_{src} = \begin{bmatrix} x_{src} \\ y_{src} \\ 1 \end{bmatrix} \tag{13}$$

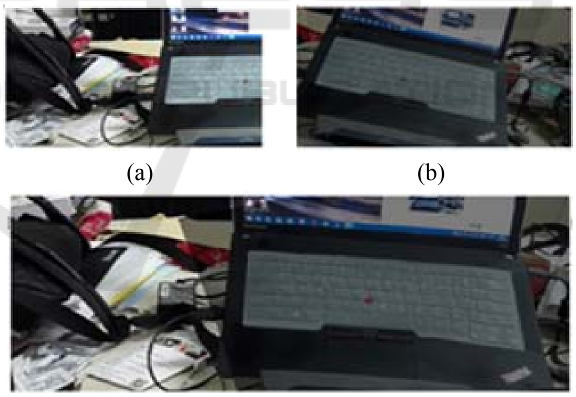

(a) (b)

(c)

Figure 4: Solution of homography: (a) original image1, (b) original image2 and (c) the image after registration.

Lowe used RANSAC algorithm to solve homography, and a good result was got. Here the RANSAC is no longer needed. We use a very small sample to get the transformation parameters between images, and find a solution that is best consistent with the parameters. With this method, we needn't set any threshold, so the processing work for different thresholds in different environment is avoided and the adaptability and automation capability of the algorithm are improved. For the color images a, b in Figure 4, we solve the homography of these two pictures through the external parameters of them, and implement the registration of these two images by matrix transformation. The result of registration is shown as picture c in Figure 4.

3 BUNDLE ADJUSTMENT

Bundle Adjustment is used to reduce the error of projected position transformation between the match points of the image to be stitched (Burt 1983). The image to be stitched is placed in a beam adjuster, and the match image which is of the largest number conformance will be the first to be adjusted. And in order to place the image to the best position for matching, the rotational transformation parameters and focus of all the images to be stitched need be adjusted to the same condition.

In this paper, we choose a projection error square algorithm which is highly robust as the objective function. Every feature point is projected into the matched image. Besides, we will minimize the square of the distance from it to the relative image. Given a map $\mathrm{u}_\mathrm{i}^\mathrm{k} \leftrightarrow \mathrm{u}_\mathrm{i}^\mathrm{l}$ ($\mathrm{u}_\mathrm{i}^\mathrm{k}$represents the position of point k in image i), its residual is calculated using (14). $\mathrm{p}_{\mathrm{ij}}^\mathrm{k}$ is the map of the point related to $\mathrm{u}_\mathrm{i}^\mathrm{k}$ from image j to image i, the process of which is described as (15).

$$r_{ij}^k = u_i^k - p_{ij}^k \tag{14}$$

$$\tilde{p}_{ij}^k = K_i R_i R_j^T K_j^{-1} \tilde{u}_j^l \tag{15}$$

Error function describes the square the sum of squared residuals generated by all images, shown as (16). And n is the total number of images. $\mathcal{L}(\mathrm{i})$ represents the image sequence matched to image i, and $\mathrm{F(i,j)}$ represents the sequence of match feature points between i mage i and image j. We use the error function Huber, shown as (17). This error function mix a formal optimization strategy that L2 is fast convergent to the domestic point (intervals less than σ), and it has good robustness of L2 to the peripheral points (intervals greater than σ).In the initialization, we make the interval of peripheral point be $\infty(\sigma = \infty)$, and let the pixel of $\sigma = 2$ in the final strategy.

$$e = \sum_{i=1}^{n} \sum_{j \in \mathcal{L}(i)} \sum_{k \in \mathrm{F}(i,j)} h(\mathrm{r}_{ij}^k) \tag{16}$$

$$h(x) = \begin{cases} |x|^2, & |x| < \sigma \\ 2\sigma|x| - \sigma^2, & |x| \geq \sigma \end{cases} \tag{17}$$

This is a problem of non-linear least squares, which is solved by Laffan Grignard algorithm. Every iteration is completed with (18), in which Φ is all the parameters and r is the residuals. For the change of parameters in covariance matrix $\mathrm{C_p}$, we need to encode its prior condition. The standard difference of angle is set to be $\sigma_\mathrm{f} = \bar{\mathrm{f}}/10$, which can help choose a proper step size to accelerate the convergence.

$$\left(\sum_{i=1}^{n} X_i X_i^T\right) u = 0 \tag{18}$$

Image registration has utilized the parameters obtained after camera calibration, but there are still unknown rotation transformations in image. Since the real camera is unlikely to be completely level and does not tilt, if we simply assume R=I for an image, there will be an impact on the final output waveform panorama. Inspired by the way of shooting panoramic images in reality, we are able to correct the waveform influence by the method of automatically stretching panorama. In actual shooting, we barely twist the camera with respect to view moment, so the camera vector X (horizontal axis) is usually located in a plane. Searching the zero vector of covariance matrix of the camera vector X, we can find its normal vector u, which is shown as (18).Because the normal vector u of a global rotational transformation is vertical, the waveform influence to the out-put image can be effectively eliminated.

4 MULTI-BAND BLENDING

We choose a multi-band blending algorithm to achieve image fusion after deep study to fusion algorithms. On the one hand, having completed the similar block segmentation in feature match section, multi-band blending can make use of it further and improve the effectiveness. On the other hand, this algorithm has been widely used and performances well in AutoStitch algorithm.

The core idea of multi-band fusion is based on the view of the dam theory. Specifically, first, the image to be stitched is divided into two parts according to its overlapping area, so that each image is divided into two parts which means four image blocks, where we only use two parts. These two parts are decomposed into different frequency bands using the Laplace transform, which is similar to scale space. With this method, two Laplace pyramids are got, and then image stitching will completed in different scales. Finally, the final image is obtained by remodeling.

Through previous work, we have got an image sequence like $\mathrm{I}^{\mathrm{i}}(\mathrm{x},\mathrm{y})(\mathrm{i}\in\{1\ldots\mathrm{n}\})$ and these imageshave been matched. This image sequence may be presented in a same coordinates $\mathrm{I}^{\mathrm{i}}(\theta,\emptyset)$. To fuse the information of different images, we set a weighted function $\mathrm{W}(\mathrm{x},\mathrm{y})=\mathrm{w}(\mathrm{x})\mathrm{w}(\mathrm{y})$ or each image, where $\mathrm{w}(\mathrm{x})$ distributes as the linear change from the center of the image to the edge of the image. Weighting function need be re-sampled in a special spherical coordinate system $\mathrm{W}^{\mathrm{i}}(\mathrm{x},\mathrm{y})$. A simple image fusion method is a weighted sum along the intensity of radiation, where the following weighting function shown as (19) is used.

$$\mathrm{I}^{linear}(\theta,\emptyset)=\frac{\sum_{i=1}^{n}\mathrm{I}^{i}(\theta,\emptyset)\mathrm{W}^{i}(\theta,\emptyset)}{\sum_{i=1}^{n}\mathrm{W}^{i}(\theta,\emptyset)} \tag{19}$$

$\mathrm{I}^{\mathrm{linear}}(\theta,\emptyset)$ is a composite spherical image by linear mixing. However, if the stitching has a slight error, this method may result in high frequent detail blur. To avoid this situation, we use a multi-band fusion algorithm proposed by Burt and Adelson[21], which fuses low-band image in a large scale and high-band in a small scale. We initial the mixed weight of the image by finding the points sequence which are of highest confidence in image i. The process is described by (20), in which $\mathrm{W}_{\mathrm{max}}^{\mathrm{i}}(\theta,\emptyset)$ represents that image i is1 at the biggest weight and 0 when other images have bigger weight. A rendered image of high throughput ate is formed in the manner of (21) and (22). In these equations, $\mathrm{g}_{\sigma}(\theta,\emptyset)$ represents the Gaussian function of standard deviation σ, and the operator $*$ denotes the convolution. $\mathrm{B}_{\sigma}(\theta,\emptyset)$ represents the spatial frequencies of the wave length in the range of $\lambda\in[0,\sigma]$ .We use a b-lend weight way to fuse the different frequency bands between images, which are shown as (23).

$$W_{max}^{i}(\theta,\emptyset)=\begin{cases}1 & if\ \mathrm{W}^{i}(\theta,\emptyset)=\arg max_{j}\,\mathrm{W}^{j}(\theta,\emptyset)\\ 0 & otherwise\end{cases} \tag{20}$$

$$B_{\sigma}^{i}(\theta,\emptyset)=\mathrm{I}^{i}(\theta,\emptyset)-\mathrm{I}_{\sigma}^{i}(\theta,\emptyset) \tag{21}$$

$$I_{\sigma}^{i}(\theta,\emptyset)=\mathrm{I}^{i}(\theta,\emptyset)*\mathrm{g}_{\sigma}(\theta,\emptyset) \tag{22}$$

$$W_{\sigma}^{i}(\theta,\emptyset)=W_{max}^{i}(\theta,\emptyset)*\mathrm{g}_{\sigma}(\theta,\emptyset) \tag{23}$$

$\mathrm{W}_{\sigma}^{\mathrm{i}}(\theta,\emptyset)$ represents the blend weight under the range of $\lambda\in[0,\sigma]$. If $\mathrm{k}\geq 1$, the following Equations are got.

$$B_{(k+1)\sigma}^{i}=\mathrm{I}_{k\sigma}^{i}-\mathrm{I}_{(k+1)\sigma}^{i}$$

$$\mathrm{I}_{(k+1)\sigma}^{i}=\mathrm{I}_{k\sigma}^{i}*\mathrm{g}_{\sigma'}$$

$$\mathrm{W}_{(k+1)\sigma}^{i}=\mathrm{W}_{k\sigma}^{i}*\mathrm{g}_{\sigma'}$$

The standard deviation of Gaussian blur function is $\sigma'=\sqrt{(2\mathrm{k}+1)}\sigma$ .This will make the later band have the same wavelength range. For each band, image sequences with overlapping areas are linearly mixed, which is shown as (24). This will result in high frequency bands are mixed in a small area, and low frequency bands are mixed in a larger context. We have selected a spherical coordinate system $\theta,\emptyset$. In principle, we can choose the two-dimensional parametric surface around any view point. And a good choice is to render to the triangle of the sphere, and reconstruct the results of blend weight in the surface of image sequence. This has great advantage to processing image sequences, and allows re-sample to another plane. But it notes that co-ordinates $\theta,\emptyset$ will have some distortion at the singularities of the poles.

$$\mathrm{I}_{k\sigma}^{multi}(\theta,\emptyset)=\frac{\sum_{i=1}^{n}B_{k\sigma}^{i}(\theta,\emptyset)\mathrm{W}_{k\sigma}^{i}(\theta,\emptyset)}{\sum_{i=1}^{n}\mathrm{W}_{k\sigma}^{i}(\theta,\emptyset)} \tag{24}$$

We have conducted some experiments to compare the multi-band image fusion algorithm with an outdoor collection of images (as the five color source images in Figure 5). For the limitations of kinect camera, the experiment did not join the collaborative stitching, which aims to illustrate the specific effects of multi-band fusion.

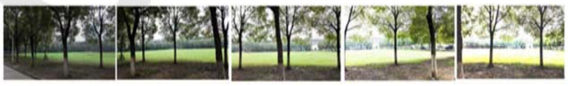

Figure 5: Color source images.

The experiment used color source images gathered outdoors with a Huawei glory 6. The image resolution was 3214×1840, and the size of the image was 1.26M. These five images were captured under different exposure and focal length whose gradients were approximately equal to each other. Figure 6 shows the results of the fusion which did not use any fusion method, and we can see a clear seam generated by the different exposures of the images. While Figure 7 shows the results of the common linear filtering fusion, the weighted average fusion algorithm. We can find the seam has been preliminary eliminated, but there are a large exposure differences between the two parts of the fused image. Because the fusion quality problems, it is difficult for this method to deal with more complex source images. And Figure 8 shows the results of multi-band fusion. The seam has been fully eliminated, and the whole image exposure is not significantly different in different regions, so the fusion is better than the simple weighted fusion.

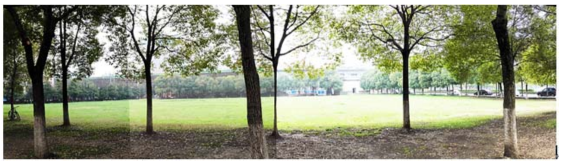

Figure 6: Fusion rendering without any fusion algorithm.

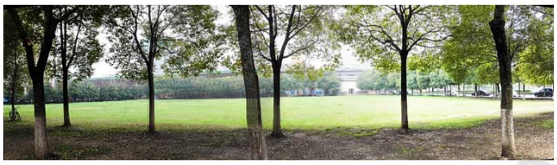

Figure 7: Fusion rendering with Linear Filtering.

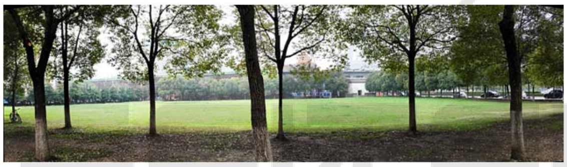

Figure 8: Fusion rendering with multi-band fusion algorithm.

5 IMPLEMENTATION AND EXPERIMENTAL RESULTS

Our experiments with different algorithms are achieved with OpenCV library under the environment of Intel Core i5 3210M CPU, 2.5GHZ, and 4GRAM. This paper mainly solves the ghost due to image registration errors and enhances the efficiency of stitching algorithm. And we select AutoStitch algorithm as the comparison algorithm.

The nine experimental images are shown in Figure 9, which are shoot with the phone (Huawei glory6) in different positions. In order to be closer to the real situation, the pixels of the nine source images are adjusted to six gradients, and the aspect ratio are roughly constant at 4:3. The pixels of the six groups of images are 480×320, 640×480, 800×600, 1140×850, 1520×1140 and 2100×1520. Since previous experiments have demonstrated the overall stitching quality of the algorithm, it is no longer to show the corresponding depth image of each image. With the proposed algorithm, firstly, the color images are divided into blocks to do extract and match of feature points with SIFT algorithm. Then, combined with the collaborative calibration, the depth information is attached to the color image and the final result of image stitching is got through RANSAC algorithm and the internal and external parameters got by camera's collaborative calibration. And the final fusion image is shown as Figure 10. And Figure 11 shows the fused image by AutoStitch algorithm.

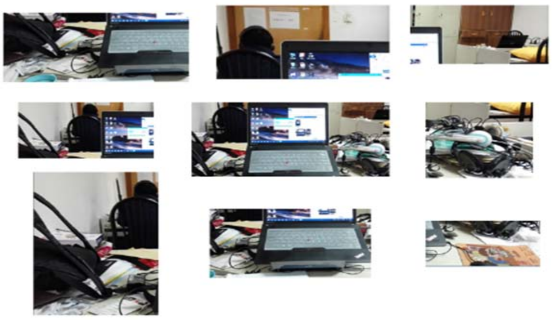

Figure 9: Experimental images gathered in lab.

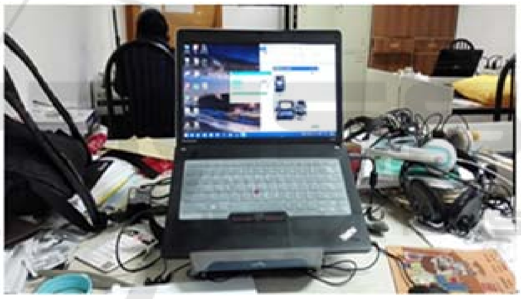

Figure 10: Seamless stitching rendering with the proposed algorithm.

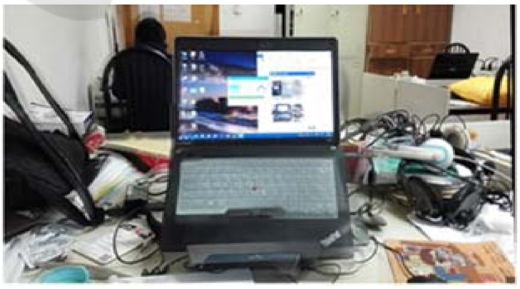

Figure 11: Seamless stitching rendering with the AutoStitch algorithm.

After a series of experiments, we select the average value as the final experimental data. A comparison of the time used in each stage between the original algorithm and improved algorithm is shown as Table 1. We can find that in the part of SIFT

Table 1: Experimental results table.

Running time（s）	Test 1		Test 2		Test 3		Test 4		Test 5		Test 6	
	Improved algorithm	AutoStitch	Improved algorithm	AutoStitch	Improved algorithm	AutoStitch	Improved algorithm	AutoStitch	Improved algorithm	AutoStitch	Improved algorithm	AutoStitch
SIFT feature extraction	1.68	1.85	1.86	2.03	3.17	3.45	4.57	4.97	6.56	7.14	8.97	9.76
Feature matching	0.67	0.92	0.68	0.93	0.67	0.92	0.67	0.92	0.67	0.92	0.67	0.92
Homography	0.03	0.09	0.04	0.09	0.04	0.08	0.04	0.08	0.04	0.08	0.04	0.08
Image stitching and correction	0.07	0.06	0.08	0.07	0.08	0.06	0.08	0.06	0.08	0.06	0.08	0.06
Image fusion	1.02	1.06	1.29	1.34	1.43	1.54	1.94	2.15	2.25	2.46	3.17	3.53
Total time	3.47	3.98	3.95	4.46	4.47	5.05	7.3	8.18	9.6	10.66	12.93	14.35

feature extraction, the SIFT algorithm based on block matching improves approximately 8% in timeliness compared to the AutoStitch feature extraction. However, compared to AutoStitch algorithm, the time consuming in feature matching of the proposed algorithm significantly reduces. This is because that AutoStitch builds KD tree for full image feature points, while the improved algorithm in this paper only builds KD tree for the feature points in overlapping area. In the part of solving homography, this paper uses the method of camera calibration, while AutoStitch uses RANSAC method. As a random sampling method, RANSAC algorithm is poor in timeliness. In image stitching and correction and image fusion, these two algorithms are not very different, so the running time is almost same.

Compared to AutoStitch algorithm, the time-consuming of improved algorithm in this paper decreases by 10%, and we can find from Table 1 that with the increase of image data, the reduction percentage in time consuming of the improved algorithm in this paper is almost unchanged. This is because that the overlapping area is bigger with the increase of image data, the proportion of which remains almost unchanged in each image with respect to the overall data.

6 CONCLUSIONS

Our research has achieved a seamless image stitching method based on depth map. The SIFT algorithm based on block matching effectively shield the non-overlapping areas, which avoids the feature points extraction and matching of the whole image and increases the efficiency of the algorithm. The collaborative calibration system based on the depth camera and color camera maps the depth data into a color image to complete registration, further increasing the quality of image stitching.

Experiments proof that the ghosting caused by shooting parallax and registration error significantly reduces. Combined with the actual needs, we select the multi-band image fusion algorithm for image fusion. Experiments to this algorithm show that the applicability of this algorithm is great. Then, we conduct a series of experiments and analysis to the seamless image algorithm based on the depth image, which increases the efficiency of stitching algorithm and reduces the ghosting.

ACKNOWLEDGEMENTS

This research work was supported by National Natural Science Foundation of China (NSFC) under grant number 61503289, Science and Technology Support Plan of Hubei Province under grant number 2015BAA120 and 2015BCE068, ESI top 1% Disciplines Foundation in 2014 (79).

REFERENCES

Jang, K.H., 1999. Constructing Cylindrical Panoramic Image Using Equidistant Matching. *Electronics Letters*, 35(20), 1715-1716.

Brown, M. & Lowe, D., 2003. Recognizing Panoramas. In *IEEE International Conference on Computer Vision.* WASHINGTON.

Lowe, D.G., 1999. Object Recognition from Local Scale-invariant Features. In *IEEE International Conference on Computer Vision.* GREECE.

Lowe, D.G., 2004. Distinctive Image Features from Scale-Invariant Key-points. *International Journal of Computer Vision,* 60(2), 91-110. Szeliski, R. & Shum, H.Y., 2000. Creating Full View Panoramic Image Mosaics and Environment Maps. *Proc Sigraph*, 251-258.

Szeliski, R. & Shum, H.Y., 2000. Creating Full View Panoramic Image Mosaics and Environment Maps. *Proc Sigraph*, 251-258.

Mikolajczyk, k. & Schmid, C., 2003. A Performance Evaluation of Local Descriptors. *IEEE Conference on Computer Vision & Pattern Recognition,* 27(10), 257.

Gholipour, A. et al., 2007. Brain Functional Localization: a survey of image registration techniques. *IEEE Transactions on Medical Imaging,* 26(4), 427-51.

Brown, M. & Lowe, D.G., 2007. Automatic Panoramic Image Stitching using Invariant Features. *International Journal of Computer Vision,* 74(1), 59-73.

Tang, Y. & Shin, J., 2010. De-ghosting for Image Stitching with Automatic Content-Awareness. *International Conference on Pattern Recognition*, 2210-2213.

Gao, J., et al., 2011. Constructing Image Panoramas using Dual-homography Warping. *IEEE Conference on Computer Vision & Pattern Recognition*, 42(7), 49-56.

Singh, R. et al., 2007. A Mosaicing Scheme for Pose-invariant Face Recognition. *IEEE Transactions on Systems Man & Cybernetics Society*, 37(5), 1212-1225.

Zou, C.M., et al., 2015. A SIFT Algorithm Based on Block Matching. *Computer Science*, 42(4), 311-315.

Umeyama, S., 1991. Least-squares Estimation of Transformation Parameters between Two Point Patterns. *IEEE Transactions on Pattern Analysis & Machine Intelligence*, 13(4), 376-380.

Chen, Q.S., et al., 1994. Symmetric Phase-only Matched Filtering of Fourier-Mellin Transforms for Image Registration and Recognition. *IEEE Transaction on Pattern Analysis & Machine Intelligence*, 16(12), 1156-1168.

Triggs, B., et al., 2000. Buddle Adjustment: A Modern Synthesis. *Vision Algorithms Theory & Practice*, 298-373.

Burt, P.J., 1983. A Mutiresolution Spline with Application to Image Mosaics. *Acm Transactions on Graphics*, 2(4), 217-236.